applied sciences

MDPI

Article

Thermal Effects on the Drilling Performance of a Limestone: Relationships with Physical and Mechanical Properties

Víctor Martínez-Ibáñez [1,*], María Elvira Garrido [2], Carlos Hidalgo Signes [2], Aniello Basco [3], Tiago Miranda [4] and Roberto Tomás [5]

1 Departamento de Ingeniería de la Construcción y de Proyectos de Ingeniería Civil, Universitat Politècnica de València, Camí de Vera s/n, 46022 Valencia, Spain
2 Departamento de Ingeniería del Terreno, Universitat Politècnica de València, Camí de Vera s/n, 46022 Valencia, Spain; egarrido@trr.upv.es (M.E.G.); chidalgo@trr.upv.es (C.H.S.)
3 Dipartimento di Ingegneria, Università degli Studi della Campania Luigi Vanvitelli, 81100 Caserta, Italy; nello.basco@live.it
4 ISISE, Department of Civil Engineering, University of Minho, 4800-058 Guimarães, Portugal; tmiranda@civil.uminho.pt
5 Departamento de Ingeniería Civil, Escuela Politécnica Superior de Alicante, Universidad de Alicante, P.O. Box 99, 03080 Alicante, Spain; roberto.tomas@ua.es
* Correspondence: vicmarib@upv.es

Abstract: This work evaluates the effect of high temperatures and cooling methods on the drillability of Prada limestone. Samples from boreholes drilled during the design stage of the Tres Ponts Tunnel in the Catalan south Pyrenean zone (Spain) were subjected to temperatures of 105, 200, 300, 400, and 600 °C, and then cooled at a slow rate or by quenching. Sievers' J-value (SJ) and brittleness (S_{20}) were determined on thermally treated samples, and the drilling rate index (DRI) was calculated for each temperature. The results show that thermal treatment implied a sustained increase in the drillability of the rock of up to 40% at 600 °C and a change in the drillability category (from medium to high). At 600 °C, SJ and S_{20} tripled and doubled, respectively, the initial values obtained for the intact rock. The results were inconclusive about the influence of the cooling method on the drilling performance of Prada limestone for the tested range of temperatures. The substantial improvement observed in the drillability of Prada limestone when heated, measured in terms of DRI, could help in the development of novel thermally-assisted mechanical excavation methods. Additionally, strong correlations between drillability variables (i.e., SJ and S_{20}) and physical and mechanical variables of Prada limestone (i.e., P- and S-wave velocities, uniaxial compression strength, elastic modulus, and Poisson's ratio) are proposed. Correlations will help make preliminary predictions of drillability based on properties such as uniaxial compression strength and ultrasound wave velocities.

Keywords: rock drillability; drilling rate index (DRI); thermal treatment; temperature; limestone; correlations

Citation: Martínez-Ibáñez, V.; Garrido, M.E.; Hidalgo Signes, C.; Basco, A.; Miranda, T.; Tomás, R. Thermal Effects on the Drilling Performance of a Limestone: Relationships with Physical and Mechanical Properties. *Appl. Sci.* **2021**, *11*, 3286. https://doi.org/10.3390/app11073286

Academic Editor: Jorge de Brito

Received: 25 February 2021
Accepted: 3 April 2021
Published: 6 April 2021

1. Introduction

Modern mechanical excavation strongly depends on the efficiency of the means involved to optimise investment costs, and so rock features must be considered [1]. Prior to excavation, the type and performance of excavation machinery (i.e., hydraulic breakers, roadheaders, shear-loaders, TBMs, drilling rigs, and cutting bits) must be determined. The influence of rock properties on drillability has been discussed by various authors. Yaşar et al. [2] experimented on cement mortar (an analogue for natural rock samples) and found that uniaxial compression strength (UCS) strongly influenced the efficiency of the drilling process in terms of specific energy increases and penetration rate decreases. Yarali and Kahraman [3] used 32 different rock types and found a strong relation between the drilling rate index (DRI) and the brittleness expressed as the area under the curve of the compressive strength-tensile strength [4]. In addition, good linear correlations were

found between DRI and UCS, Brazilian tensile strength (BTS), shore scleroscope hardness, and axial and diametral point load strength (PLT) [5,6]. Saeidi et al. [7] studied 38 in situ drillings in porphyry andesite, limestone, and sandstone, and found that the UCS of rock, the vertical pressure on bit, and bit rotational speed were the most significant parameters in the penetration rate for rotary drilling. Özfırat et al. [8] experimented on 42 rocks of different types and found that DRI showed strong correlations with UCS and BTS. Yetkin et al. [1] used schist samples and found a strong relationship between DRI, UCS, BTS, Schmidt hardness (SH), instantaneous cutting rate (ICR), unit weight, rock mass rating (RMR), and the Cerchar abrasiveness index (CAI). Capik et al. [9] used 43 samples from different types of rocks and determined that DRI decreased with increasing UCS, PLT, BTS, and SH, and that DRI increased with apparent porosity and void ratios. More recently, Yenice [10] found better predictions of DRI from UCS and BTS for hard rocks (UCS > 100 MPa) than for soft rocks.

Elastic and plastic deformations occur during drilling, and for that reason the effects of elastic properties have also been studied in terms of drilling aspects by different authors. Jamshidi et al. [11] used artificial neural networks to estimate UCS and elastic modulus (using operational drilling parameters from oil wells in Iran as inputs) and determined that both UCS and elastic modulus are strongly correlated with operational drilling parameters, although UCS showed the best coefficients of determination (demonstrating that UCS has a greater effect in drilling performance than elastic modulus). Ataei et al. [12] studied 11 drilling sites from a mine in Iran and showed a good relationship between drilling rate (DR) and UCS, P-, and S- wave velocities. Su et al. [13] experimented on samples from nine different rocks and found a strong correlation between DRI and UCS. Although correlation between DRI and elastic modulus was poor, a correlation between Sievers' J-value (SJ) and elastic modulus was found.

Previous research evidence shows that mechanical and physical properties strongly determine the drilling performance of rocks, and such properties show the dramatic variations with temperature and cooling method that condition the drillability of thermally treated rocks. Thermal effects on the physical, mineralogical, and mechanical properties of rocks are of interest to researchers. Moreover, the degree of thermal damage strongly depends on the type of rock, and more than a quarter of the studies on the thermal response of rocks are specifically focused on limestones [14]. Lion et al. [15] observed a decrease in UCS even at low temperatures (T < 250 °C). Yavuz et al. [16] described a marked decrease in bulk density, P-wave velocity, and effective porosity at 400 °C. Franzoni et al. [17] reported an increase in open porosity, as well as water absorption and reduction in mechanical properties when heating limestones up to 400 °C, as a consequence of the anisotropic thermal deformation of calcite crystals. Brotóns et al. [18] reported an increased variation in the physical and mechanical features of carbonate rocks when cooled by water immersion. Andriani and Germinario [19] observed a clear reduction in uniaxial compression strength (UCS) from 500 °C on calcareous and dolomitic rocks from Apulia in Italy, with temperatures above 600 °C usually marking a dramatic decline in UCS [20,21] Beck et al. [22] explored colourimetry to determine thermal damage in buildings and described a trend of limestone to redden (later confirmed in Prada limestone and related to oxidation of iron compounds) [23]. Natural limestone becomes lighter in appearance with increasing temperature [23,24]. Zhang et al. [25] determined that from 200 to 500 °C porosity and pore size rapidly increase, and from 500 to 600 °C UCS, elastic modulus, Poisson's ratio, and hardness decreased. Later, Zhang and Lv [26] described a strong relationship between mineral content and thermal damage in limestones (China). Martínez-Ibáñez et al. [23] described a significant contribution of the thermal oxidation of pyrites in the explosive behaviour and thermo-chemical damage of Prada limestone from 400 °C. Martínez-Ibáñez et al. [27] identified micro-structural changes produced by high temperatures and cooling methods in Prada limestone, and related them with severe variations in the physical and mechanical features of this type of rock. Such dramatic changes are mainly explained by the anisotropic expansion of calcite [15,28], and by other

physicochemical processes such as the mismatch in thermal expansion coefficients between mineral particles [29] and the quartz phase transition [30,31]. The greater thermal damage in water-cooled samples is due to tensile stresses that nucleate cracks [32].

Current drilling methods are based on mechanical abrasion, and this produces substantial drill bit wearing and low rates of penetration in hard rocks, resulting in high drilling costs [33,34]. Therefore, researchers aim to improve drilling performances using emerging drilling technologies, and one alternative approach is to thermally assist conventional rotary drilling by heating the rock. Rossi et al. [35] explored the feasibility of thermally assisted drilling using a flame jet to achieve high local heating rates, and determined a drop of 30% in UCS for temperatures up to 600 °C. Jamali et al. [36] used high powered laser technology to decrease rock strength, drilling strength, and fracture toughness at rates of 60% in granite and 30% in sandstone. Rossi et al. [37] studied a combined thermo-mechanical drilling (CTMD) using a flame jet and stated that the thermal treatment of rocks causes extensive thermally induced cracks in granite and sandstone, which significantly enhances the penetration performance of cutting tools. Later, Rossi et al. [38–40] implemented this technology in the field and demonstrated an increase in the removal performance in hard rocks by up to a factor of three when compared to conventional drilling methods, and concluded that integration of thermal assistance to conventional rotary drilling constitutes an interesting approach to facilitate the drilling process.

DRI [41] is among the most used testing methods to determine the drillability characteristics of rock. NTNU/SINTEF registered as trademark the DRI test [42], which is assessed on the basis of two laboratory tests, the brittleness value (S_{20}) test [43] and Sievers' J-value (SJ) miniature drill test [44]. In this study, SJ and S_{20} tests were performed on thermally treated samples from two boreholes drilled during the design stage of the Tres Ponts Tunnel in Prada limestone to determine drilling rate index (DRI) variation with temperature. Thermal treatment effects on Prada limestone drillability would help improve the efficiency of mechanical excavation. Prediction of penetration rates for rotary drill rigs is of great importance in mine and tunnelling scheduling [44–47]. Using prediction equations enable selecting the drilling rig type best suited for certain conditions [48]. We explore correlations to predict the SJ and S_{20} of thermally treated limestone from P- and S-wave velocities, UCS, elastic modulus, and Poisson's ratio. Such correlations would help make preliminary predictions of the variation in SJ, S_{20}, and DRI of Prada limestone from: (a) other properties whose determination is quicker and easier; (b) non-destructive laboratory tests (i.e., ultrasound wave velocity); or (c) from more common test procedures (e.g., the uniaxial compressive test).

2. Materials and Methods

Prada limestone is a Lower Cretaceous formation located in the Serra de Prada, a range of mountains in the southern Pyrenees (Lleida province, Spain). Rock samples were taken from two horizontal boreholes drilled during the design stage of the Tres Ponts Tunnel, which is planned to be entirely excavated from Prada limestone in the municipalities of Organyà and Fígols, close to a narrowing of the Segre river as it passes next to the Serra de Prada, in an area known as the Congost de Tres Ponts. The tunnel will be oriented north-south on the C-13 road, measures 1273 m in length, and its maximum depth from the ground surface will be of 285 m. Figure 1 shows the area of study including the Serra de Prada, Congost de Tres Ponts, the Tres Ponts Tunnel, and the position and spatial coordinates of the two horizontal boreholes.

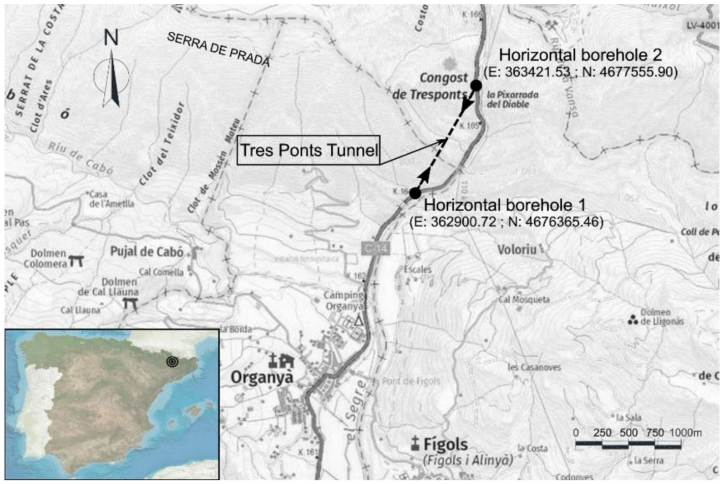

Figure 1. Location of the Tres Ponts Tunnel in the Congost de Tresponts area. Borehole coordinates are expressed in meters in the UTM 31N/ETRS 89 reference system. Image modified from Institut Cartogràfic i Geològic de Catalunya (www.icc.cat accessed on 25 February 2021).

Samples were very homogeneous and only presented changes in the grey tone and very thin veins of calcite (Figure 2). The effects of high temperatures in textural, physical, and mechanical features from the Prada formation were described in previous research [27]. A dark grey fraction from Prada limestone exhibited an increased thermal damage and explosive behaviour when heated to above 400 °C, and this is related to an increase in the pore pressure caused by SO_2 released during the thermal oxidation of pyrites [23]. Due to such different effects produced by the thermal treatment, the dark grey fraction was separated from the rest of samples and was not considered in this research.

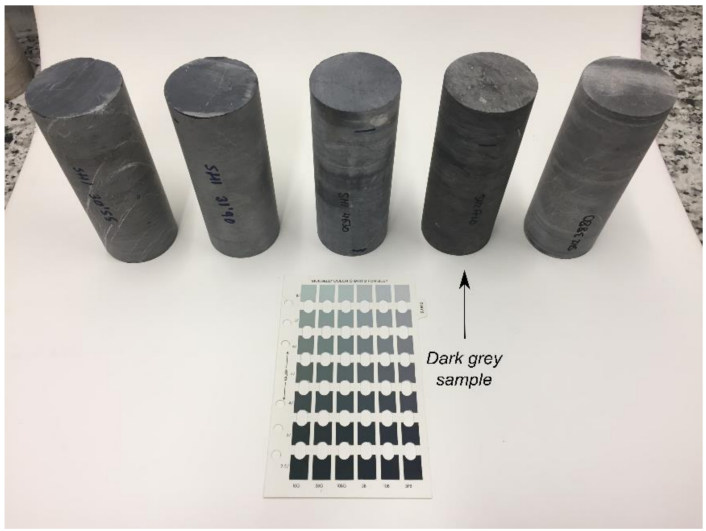

Figure 2. Changes in the grey tone and very thin veins of calcite observed in the intact samples. A dark grey texture was separated from the rest of samples and does not form part of this research.

Optical microphotographs (Figure 3) enabled Prada limestone to be identified as a grainstone or biosparite with abundant bioclasts, where cement is abundant and mainly consists of crystalline mosaics of calcite spar that fill the interparticle porosity. Micritic matrix is minor and irregularly distributed, and discontinuities are abundant and consist of fissures, calcite veins, and a small number of stylolites. Some angular and sub-angular grains of monocrystalline quartz, and sub-rounded grains of iron sulphides dispersed in the rock matrix appeared in a minor proportion.

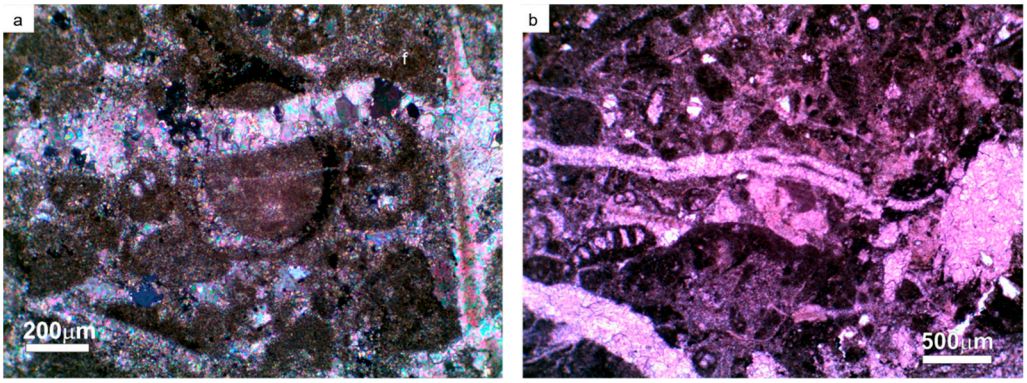

Figure 3. Optical microphotographs of intact Prada limestone. Bioclasts and micritic matrix cut by calcite veins (**a**). Detail of molluscs (**b**). Microphotographs were taken under parallel-nicols.

A temperature of 105 °C was applied to a total of 110 samples to remove moisture and these are considered references for the determination of intact rock properties. The average initial values for physical and mechanical properties of the intact rock are summarised in Table 1. Subsequently, five groups of 20 samples were separated and heated in an electric furnace at a slow rate (a gradient of 5 °C/s was applied) to target temperatures of 200, 300, 400, 500, and 600 °C. Target temperatures were then maintained for one hour. Heated specimens at each target temperature were then separated into two groups of five samples and cooled by one of two methods: (i) at a slow rate to room temperature of 21 °C; or (II) by quenching through water immersion, according to the procedure described by Brotóns et al. [18]. Temperatures inside the furnace were monitored with a PicoLog 6 data logger. Figure 4 illustrates the number of laboratory tests performed for each temperature and the number of samples used in this research methodology.

Table 1. Reference values for intact samples heated at 105 °C.

Parameter	Min.	Max.
Dry unit weight, ρ_d (kN/m^3)	26.59	27.09
Open porosity, n_e (%)	0.67	1.75
P-wave velocity, V_p (km/s)	5.30	5.41
S-wave velocity, vs. (km/s)	2.63	2.67
Uniaxial compressive strength, σ_{ci} (MPa)	140.86	188.40
Elastic modulus, E (GPa) (from mechanical tests)	71.15	84.23
Poisson's ratio, ν (from mechanical tests)	0.26	0.36

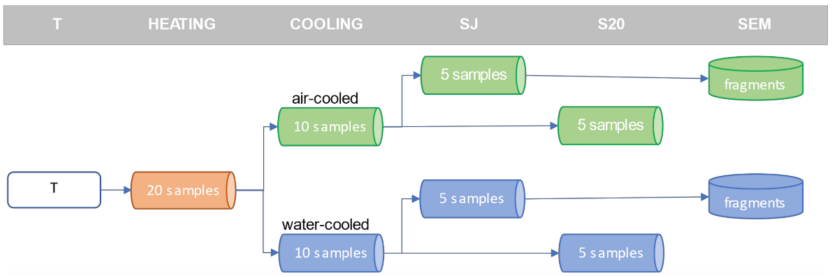

Figure 4. Methodological scheme of the laboratory tests and the number of samples tested. The tests performed at each temperature (T) are: Siever's J drillability value (SJ); brittleness value (S_{20}); and microstructure by scanning electron microscopy (SEM).

Optical and scanning electron microscopy (SEM) in backscattered electron mode was used to study the petrographic features of representative samples from Prada limestone. Sample surfaces were polished with alumina and diamond powder; the finest abrasive

used was a 0.4 µm diamond powder. Uncovered polished surfaces were studied in a Hitachi S-3000 N variable pressure SEM working in a low vacuum, and salt tested surfaces were analysed in a high vacuum SEM in secondary electron mode.

Sievers' J-miniature drill test measures rock surface hardness or resistance to indentation. Figure 5a shows the laboratory equipment used in this research to determine SJ value according to Bruland [41], which is defined as the measured drillhole depths after 200 revolutions of the 8.5 mm miniature drill bit (Figure 5b) acting with a vertical load of 20 kg. A total of 55 samples (five samples from each temperature and cooling method) were chosen to perform Sievers' J-miniature drill test. The test was repeated five times on each rock sample, and the Sievers' J-value was calculated as the mean value of the depth of the miniature drill holes, measured in 1/10 mm according to Bruland [41].

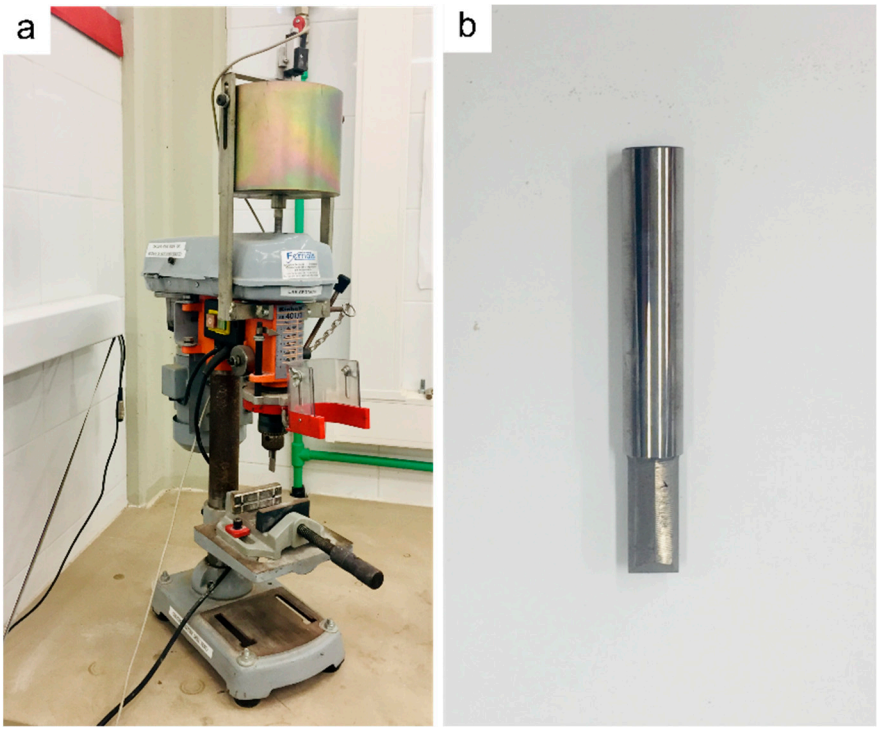

Figure 5. Laboratory equipment for Sievers' J-miniature drill test (**a**) and miniature drill bit (**b**) used in this research.

The brittleness test gives a good measure of the rock brittleness or the ability of the rock to resist crushing by repeated impacts. The test was conducted according to Bruland [41], so a total of 500 g of aggregate in the fraction 11.2–16.0 mm was prepared from each sample. The aggregate was then crushed by 20 impacts in the mortar and then the value S_{20} was expressed as the percentage of material passing through the 11.2 mm sieve (Figure 6). The test was conducted on 55 samples (five samples from each temperature and cooling method), and the brittleness S_{20} value for each temperature was taken as the mean value of the samples tested.

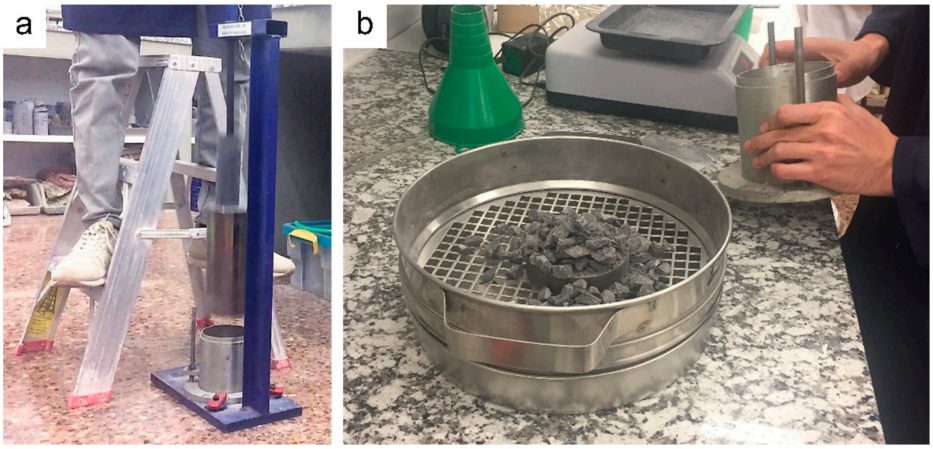

Figure 6. Crushing of the aggregate in the mortar (**a**) and determination of the percentage of material passing through the 11.2 mm sieve (**b**).

3. Results

3.1. Effects of Temperature on the Micro- and Macro-Structural Features

Variations in the micro- and macro-structural features of Prada limestone with temperature were already documented in detail in previous research [27], where SEM and MIP analyses refer to thermal treatment as a cause for dramatic micro-structural changes in Prada limestone in terms of porosity and micro-crack growth and coalescence. New SEM performed in this study confirms the presence of trans-granular fissures and porosity when heated to 400 °C (Figure 7a), and well-formed and connected fissures developed at 600 °C (Figure 7b), both in water-cooled samples. The macro-structural effects of temperature involve visible fissure growth, splitting, and cracking (Figure 8). Such effects were noticeable from 400 °C and were more severe with increasing temperature.

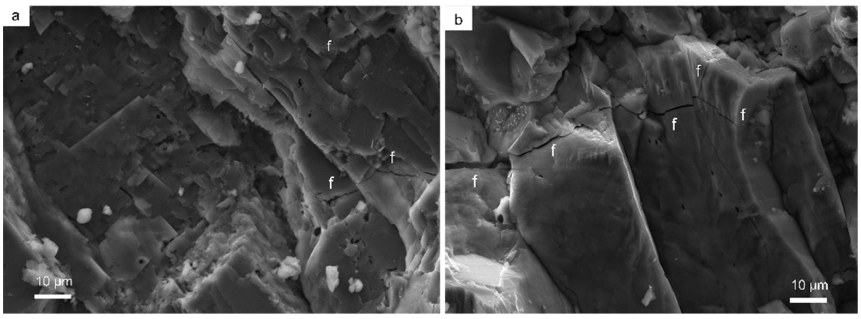

Figure 7. SEM images showing fissures (f) for samples heated to 400 °C (**a**) and 600 °C (**b**) and then water-cooled. An increase of 2000× was used for all figures.

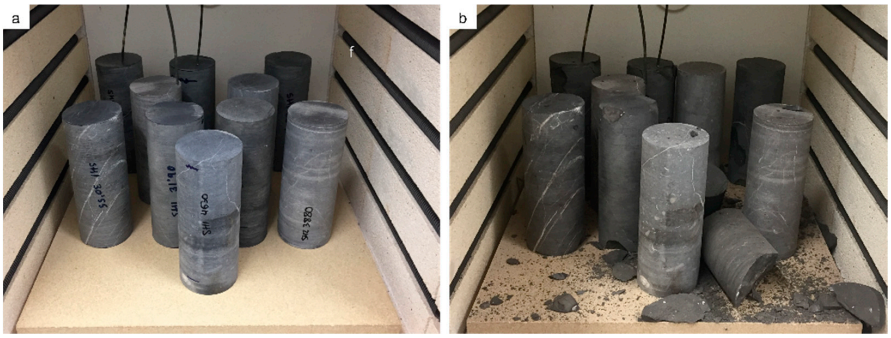

Figure 8. Samples before (**a**) and after (**b**) heated to 600 °C. Effects of temperature involve visible fissure growth, splitting, and cracking.

3.2. Drillability Variation with Temperature

Mean and standard deviation numerical values of SJ and S_{20} are depicted in Table 2 and evolution for the different temperatures are represented in Figure 9. The results show significant values of standard deviation at certain temperatures related to the perceived slight variations in the visual appearance of samples (i.e., changes in the grey tone and presence of very thin calcite veins).

Table 2. Variation with temperature of Siever's J miniature drillability test (SJ), brittleness test (S_{20}), and drilling rate index (DRI) final value and for air- and water-cooled samples.

	Air-Cooled Samples				Water-Cooled Samples			
Temperature (°C)	**SJ (1/10 mm)**	**S_{20} (%)**	**DRI**	**Class**	**SJ (1/10 mm)**	**S_{20} (%)**	**DRI**	**Class**
105	11.35 ± 4.41	42.77 ± 10.94	44	Medium	11.35 ± 4.41	42.77 ± 10.94	44	Medium
200	14.92 ± 6.27	45.12 ± 8.40	49	Medium	5.73 ± 0.71	39.23 ± 6.02	39	Low
300	10.30 ± 7.05	44.23 ± 7.41	45	Medium	14.66 ± 5.97	41.73 ± 7.26	45	Medium
400	17.29 ± 10.66	49.45 ± 5.67	52	Medium	14.56 ± 9.02	48.16 ± 2.18	50	Medium
500	16.34 ± 10.70	55.84 ± 6.07	59	High	21.88 ± 5.60	57.71 ± 4.74	62	High
600	30.13 ± 11.32	56.43 ± 4.44	62	High	23.60 ± 9.81	55.89 ± 9.87	62	High

SJ for air-cooled samples showed little variation up to 500 °C, and then we observed a sudden increase at 600 °C that tripled the initial mean values of the intact rock. Water-cooled samples showed a constant increase with temperature except for a marked local decrease at 200 °C. Final mean values at 600 °C doubled the initial values of the intact rock. Values of S_{20} for air-cooled samples were almost constant up to 300 °C. Values then increased for 400 °C and 500 °C, and remained constant at 600 °C (where a final mean value of 1.3 times that for intact rock was reached). Slight differences were registered between air- and water-cooled samples up to 400 °C where water-cooled samples showed lower values especially at 200 °C. For higher temperatures, trends were almost equal for both cooling methods.

Values of SJ and S_{20} were combined to obtain a final DRI value for each temperature (Figure 9c), and this enabled classification of the drillability of Prada limestone (Table 2) according to Bruland [41]. DRI increased with temperature, and this implied a change in the drillability category at 500 °C (from medium to high) for both cooling methods. Decreases in the DRI could be observed at 200 °C for water-cooled samples, which is consistent with the recorded variations in SJ and S_{20}. No relevant differences could be observed between cooling methods for the highest temperatures.

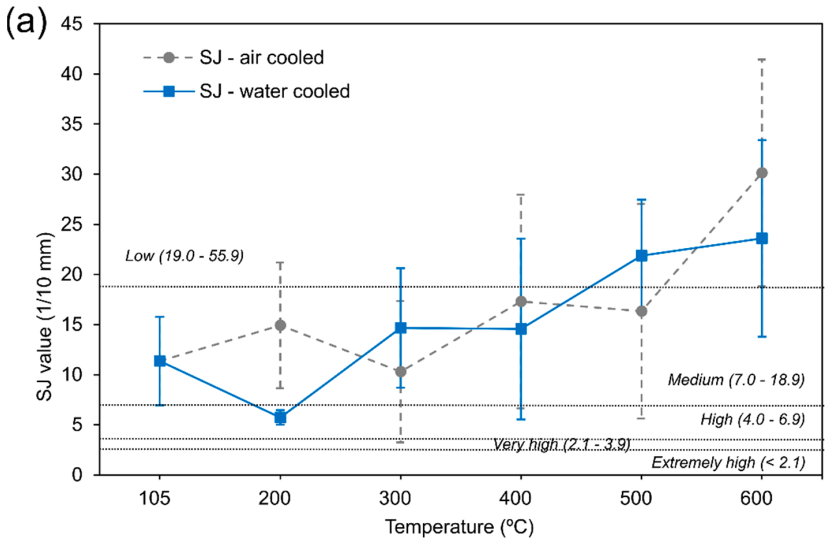

Figure 9. *Cont.*

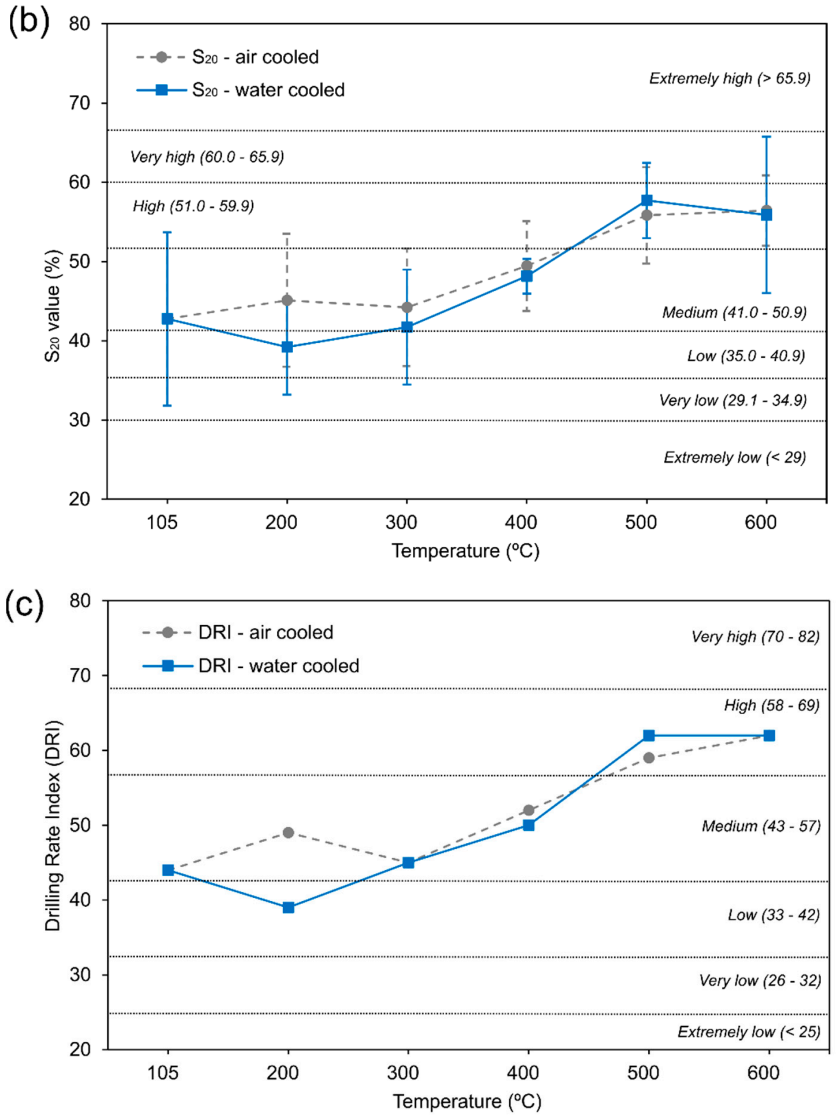

Figure 9. Variation with temperature of Siever's J miniature drillability SJ (**a**), brittleness S_{20} (**b**), and drilling rate index (**c**) for air- and water-cooled samples. Categories have been represented for Sj and S_{20} according to Dahl et al. [49], and for DRI according to Bruland [41].

3.3. Correlations between Parameters

Correlations have been proposed in this work to predict the variation in the drillability with temperature from variations in the physical and mechanical propertiesfor both air and water-cooled samples. Properties correlated in this study are obtained from different fragments within the same samples, which prevents providing pairs of values for the same fragments. This is because drillability tests performed here are destructive, and therefore it is not possible to make other tests such UCS on the same rock specimens. In other words, since DRI and UCS tests are destructive, for each temperature they are performed using different fragments (whose values are averaged and then correlated). Thus, regression curves are calculated using the mean values of each property determined at each temperature in line with other authors [10,27,50] since the pairs of correlated values of each sample that define the scatter cannot be considered for adjusting such functions. Different correlation functions exist between SJ, S_{20}, and other physicomechanical parameters of the intact rock, but they do not refer to thermally treated samples. This research novelty explores the variation in SJ and S_{20} with temperature, and their correlation with other physicomechanical features in a thermally treated rock. To provide the most accurate

predictions of drillability parameters for making preliminary decisions about the drilling process (e.g., drilling rig type and excavation process), we propose correlations to explore the best fitting functions based on coefficients of determination (Table 3), and we evaluate their suitability based on residuals and absolute relative errors (Table 4). We also discuss if correlations can provide reference values for the drillability features of thermally treated rocks, and so we consider valid those correlations providing coefficients of determination greater than 0.80 and relative errors smaller than 10%.

Table 3. Coefficients of determination (R^2) for simple regression curves studied to predict SJ and S_{20} from mechanical and normalised (N) physical parameters (UCS, elastic modulus, Poisson's ratio, P- and S-wave velocities).

Cooling Method	Parameter	R^2 for SJ Predictions				R^2 for S_{20} Predictions			
		Linear	Exponential	Logarithmic	Power	Linear	Exponential	Logarithmic	Power
Air	UCS	0.74	0.79	0.87	0.89	0.71	0.73	0.69	0.70
	Elastic modulus	0.56	0.61	0.55	0.59	0.96	0.96	0.93	0.92
	Poisson's ratio	0.76	0.77	0.86	0.84	0.90	0.89	0.84	0.83
	P-wave velocity	0.65	0.64	0.69	0.66	0.92	0.91	0.90	0.89
	S-wave velocity	0.74	0.71	0.77	0.72	0.89	0.88	0.86	0.84
Water	UCS	0.63	0.43	0.72	0.51	0.69	0.67	0.77	0.75
	Elastic modulus	0.76	0.66	0.78	0.64	0.80	0.79	0.85	0.84
	Poisson's ratio	0.85	0.69	0.80	0.62	0.90	0.89	0.83	0.81
	P-wave velocity	0.80	0.62	0.82	0.63	0.88	0.87	0.89	0.88
	S-wave velocity	0.82	0.64	0.81	0.62	0.91	0.90	0.88	0.86

Table 4. Average residuals and relative errors for predictions of SJ and S_{20} from physical and mechanical variables at the highest temperatures (400, 500, and 600 °C).

Cooling Method	Parameter	SJ Predictions		S_{20} Predictions	
		Average Residuals (1/10 mm)	Average Relative Errors (%)	Average Residuals (1/10 mm)	Average Relative Errors (%)
Air	UCS	1.48	6.97	3.15	5.84
	Elastic modulus	5.04	23.70	0.93	1.71
	Poisson's ratio	1.99	9.35	1.69	3.10
	P-wave velocity	4.31	20.26	1.58	2.93
	S-wave velocity	3.68	17.33	1.65	3.37
Water	UCS	0.90	4.48	2.87	5.33
	Elastic modulus	2.23	11.16	2.95	5.34
	Poisson's ratio	1.05	5.26	1.99	3.72
	P-wave velocity	0.19	0.96	1.96	3.64
	S-wave velocity	0.39	1.97	2.04	4.28

In general, the best fitting functions for SJ were logarithmic, while linear functions showed best results for S_{20} correlations for most parameters and cooling methods (Table 3). Coefficients of determination were higher in the case of S_{20} predictions for almost all regression functions and parameters.

The best correlation functions derived from Table 3 have been plotted to discuss trends. Thus, predictions from mechanical variables (UCS, elastic modulus, and Poisson's ratio) are represented for SJ in Figure 10 and for S_{20} in Figure 11. Predictions from physical variables (P- and S-wave velocities) are depicted in Figure 12 for SJ and in Figure 13 for S_{20}. Residuals have been also plotted as the differences between values measured in laboratory tests and predicted from regression functions. To evaluate the quality of predictions, absolute residuals and absolute relative errors have been represented for the average temperatures where DRI exhibited greatest variation (400, 500, and 600 °C) (Table 4).

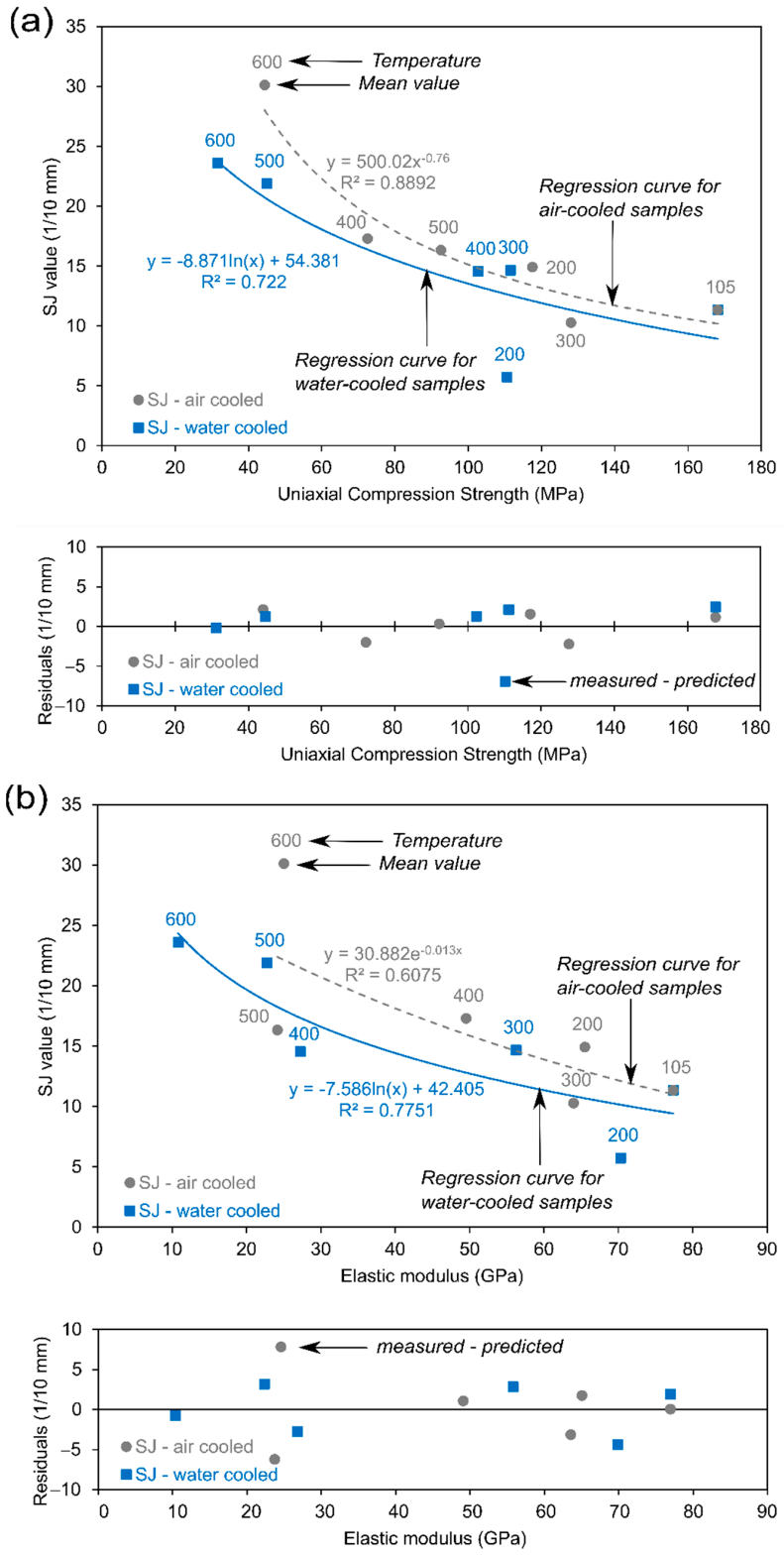

Figure 10. *Cont.*

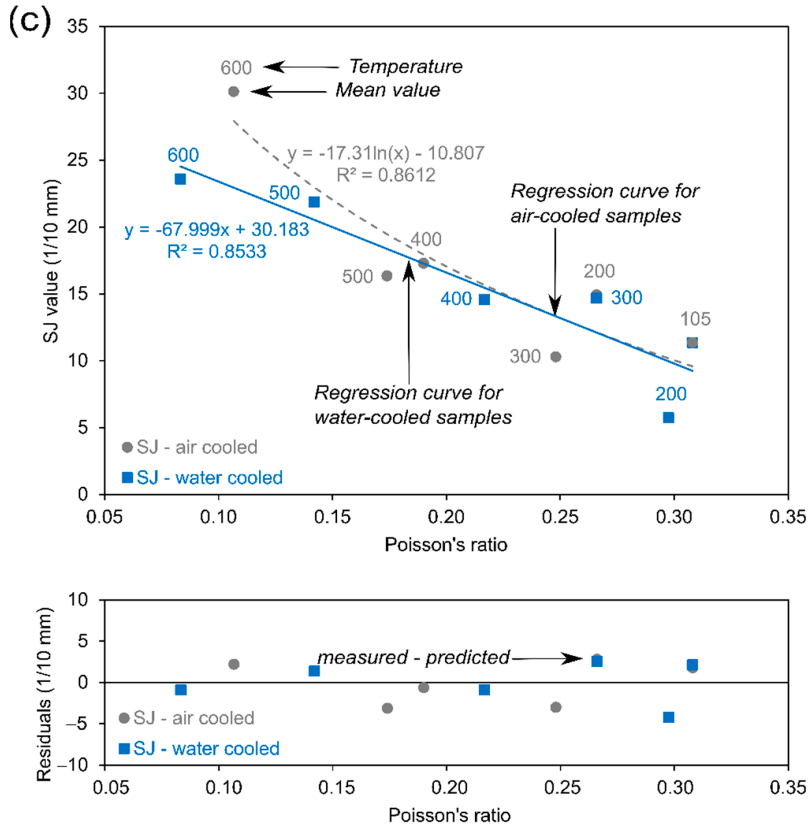

Figure 10. Correlations between variation of SJ and: (**a**) UCS; (**b**) elastic modulus; and (**c**) Poisson's ratio for air- and water-cooled samples.

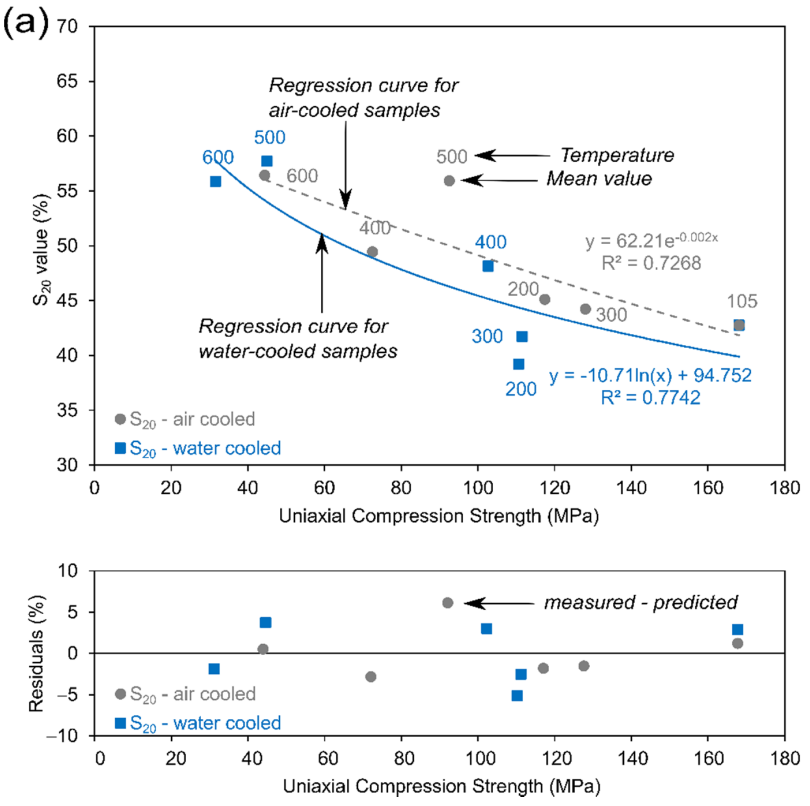

Figure 11. *Cont.*

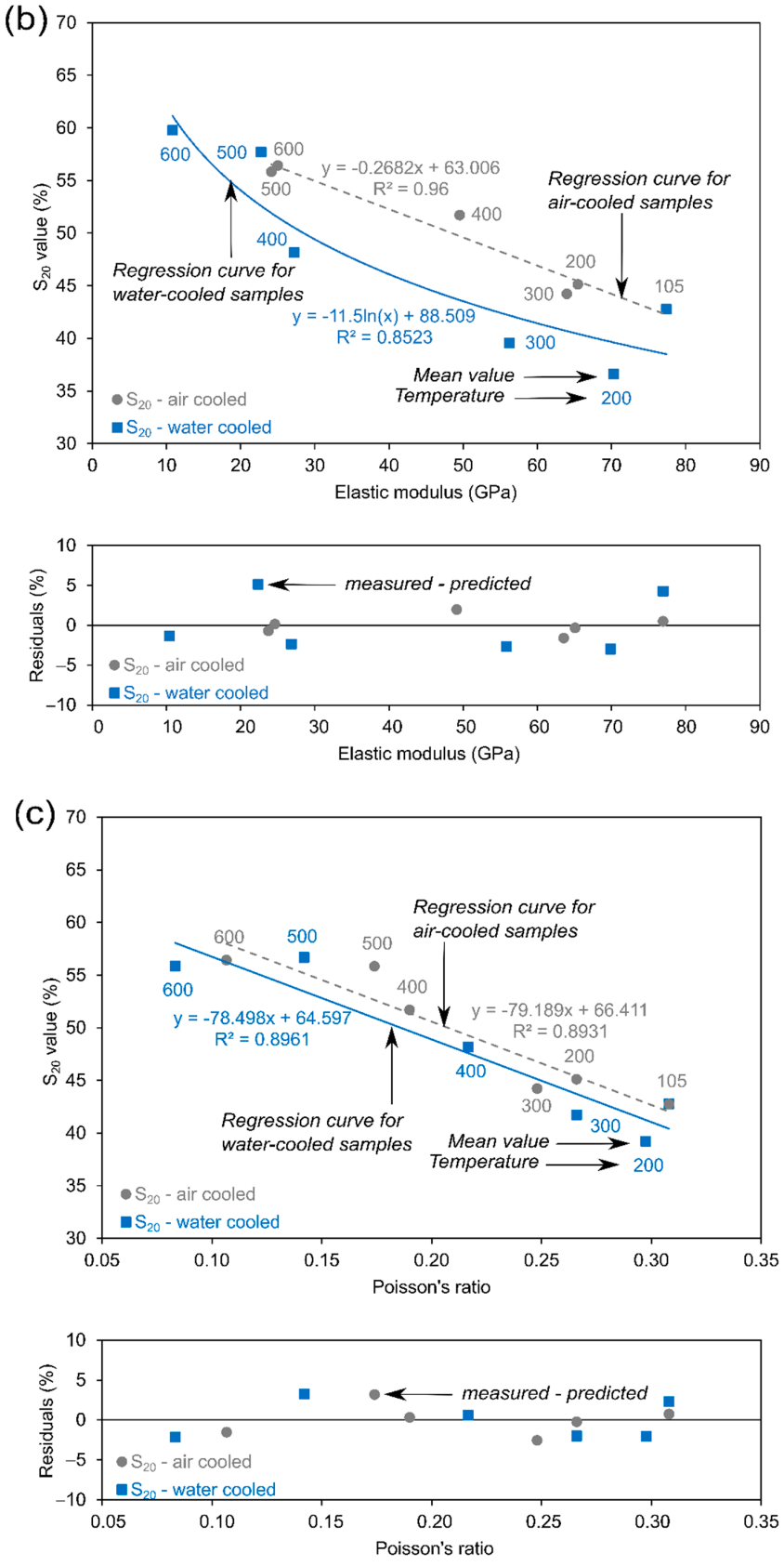

Figure 11. Correlations between variation of S_{20} and: (**a**) UCS; (**b**) elastic modulus; and (**c**) Poisson's ratio for air- and water-cooled samples.

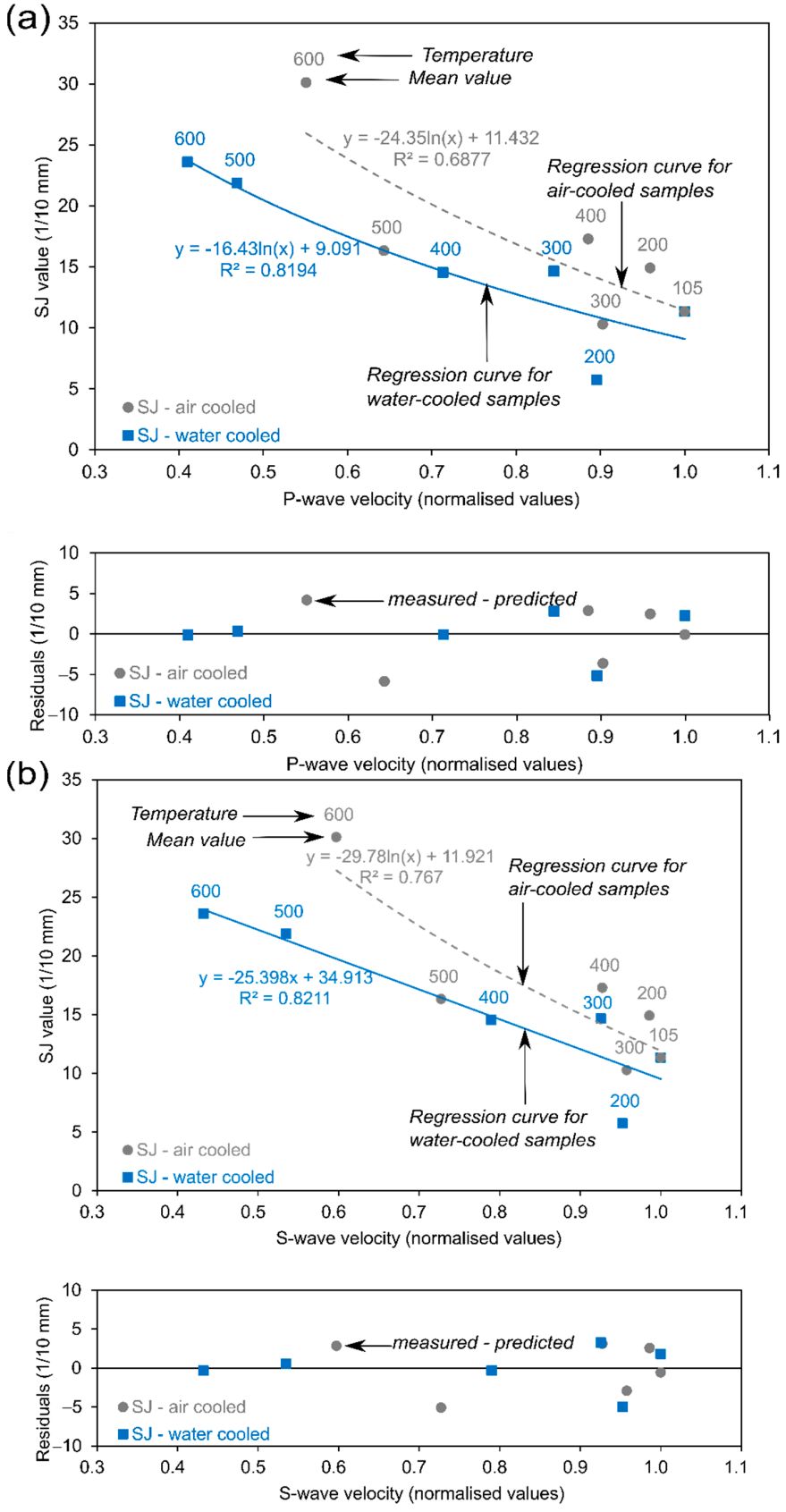

Figure 12. Correlations between variation of SJ and (**a**) P- wave velocity; and (**b**) S-wave velocity for air- and water-cooled samples.

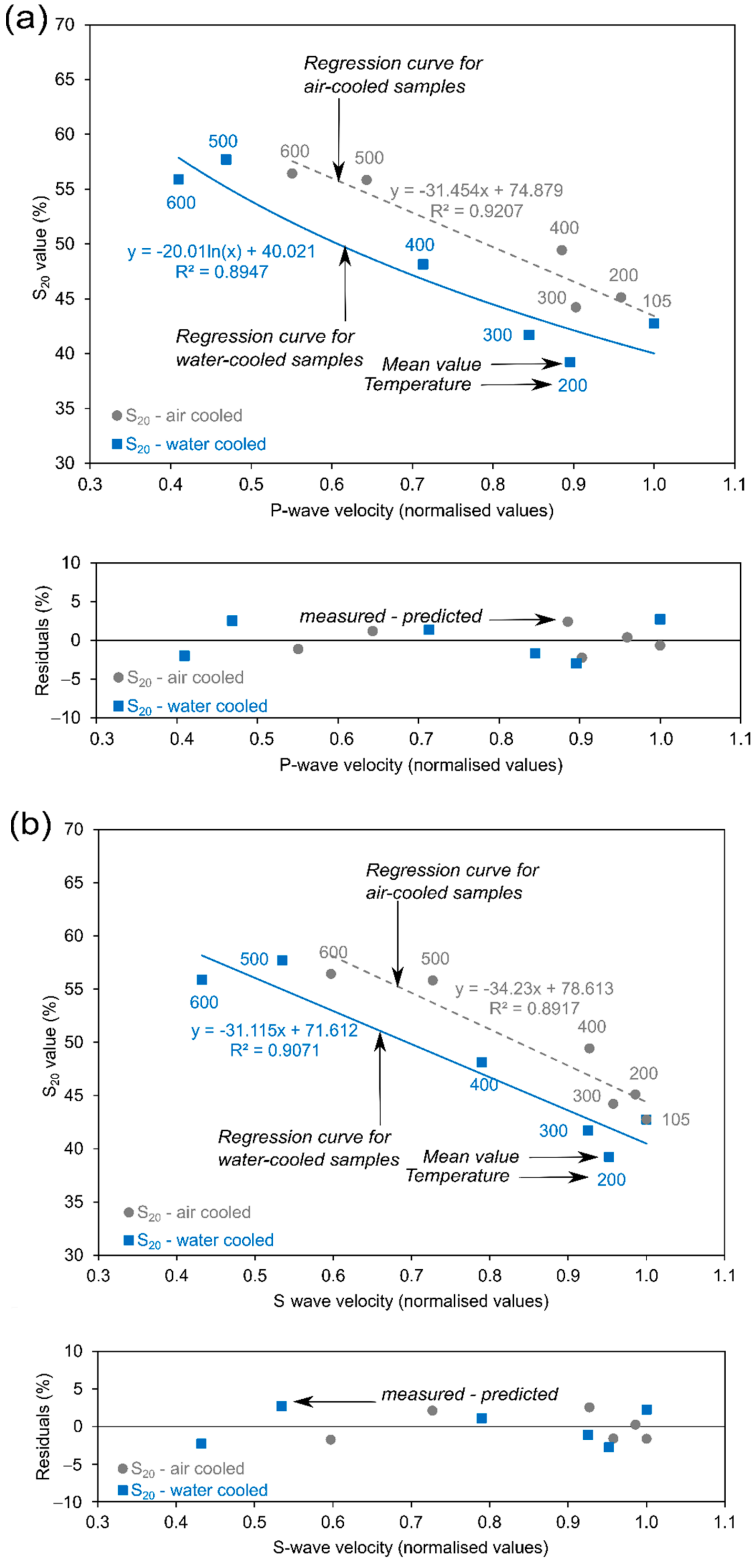

Figure 13. Correlations between variation of S_{20} and P- (**a**) and S-wave velocity (**b**) for air- and water-cooled samples.

4. Discussion

Decay in mechanical (UCS, elastic modulus, and Poisson's ratio) and physical (P- and S-wave velocities) properties were accompanied with a general increase in the Siever's J-

value and in the brittleness S_{20} value that, together with the DRI index, point to a sustained increase in Prada limestone drillability.

DRI, SJ, and S_{20} values for the Prada intact limestone (before thermal treatment) have been compared with three types of intact limestones studied by Yarali and Soyer [5]. Although those limestones presented high, or very high, drillability categories, a lower DRI in Prada limestone (DRI = 44 corresponding to a 'medium drillability' class) is attributed to a greater UCS. Indeed, a linear correlation between UCS and DRI was proposed by Yarali and Soyer [6] for intact limestones. This type of correlation has proven an excellent prediction of DRI from UCS for intact Prada limestone (UCS = 168.09 MPa; DRI = 43.71). In the case of SJ, we obtained a value of 11.35 ± 4.41 1/10 mm for the intact Prada limestone, and this corresponds to medium surface hardness, or resistance to indentation, according to the classes proposed by Dahl et al. [49]. In the case of S_{20} we obtained a value of 42.77 ± 10.94% for the intact rock and this is consistent with a medium rock brittleness, or the ability to be crushed by repeated impacts (also according to Dahl et al.) [49].

Thermal treatment resulted in a total increase of 40% in the DRI of Prada limestone at 600 °C, with no significant differences between cooling methods for the studied range of temperatures. Research is scarce on the variation of DRI with temperature, and so results cannot be compared with other lithologies. Research is scarce on the variation of DRI with temperature and so results cannot be compared with other existing experiences. Methodologies and variables considered in the existing research on thermally assisted drilling differ greatly from those presented in our research. Rossi et al. [35] reported a drop of 30% in the UCS of sandstone and granite for temperatures at 600 °C when using a flame jet to achieve high local heating rates, and UCS is strongly related to the drillability of the rock [11–13]. Although such a decrease in drillability is in the same range as that observed in our research, the lithologies and heating rates (20 °C/s) are very different. Jamali et al. [36] applied high powered laser technology and performed scratch tests to indirectly measure reductions in rock strength, drilling strength, and fracture toughness at rates of 60% in granite and 30% in sandstone, but such results cannot be directly compared to the DRI reduction observed in our research, because the achieved temperatures and applied heating rates cannot be deduced. A decrease in the DRI with temperature for water-cooled samples coincided with a marginal porosity and a volume decrease at 200 °C [51]. This effect is related to the closure of pores and fissures by thermal dilation of calcite [16,52] and is a factor that hinders penetration [37]. Thus, closure of pores and fissures is behind a decrease in thermal drilling performance at low temperatures for water-cooled samples.

SJ and S_{20} represent different effects in a rotary-percussive drilling process, since the impact action of the bit is expressed by S_{20}, whereas thrust and rotation match with the SJ value [13], and so we study their respective variations with temperature separately. Temperature influence is remarkable because for the highest temperature of 600 °C, SJ tripled and S_{20} doubled the initial values of the intact Prada limestone. The category of brittleness, or the ability to be crushed by repeated impacts (measured by S_{20}), varied with temperature from medium to high, and rock surface hardness or resistance to indentation (represented by SJ) varied from medium to low (both in the scale of Dahl et al.). We attribute this effect to the increase of porosity and the propagation and coalescence of micro fissures due to thermal treatment. That is noticeable in the case of S_{20}, where the trend is consistent with microstructural changes due to thermal treatment [27]. Incipient trans-granular fissures and porosity developed when heated to 400 °C match a gentle increase in S_{20}. At 500 °C the pore-sizes increase and fissures were larger and more connected, in agreement with a marked increase in crushability by repeated impacts represented by S_{20}.

It is noteworthy that at 600 °C, SJ values were smaller for water-cooled samples, and S_{20} values were equal for both cooling methods. These results contradict the general observed trend of greater decay in mechanical and physical parameters when cooling with water for the studied range of temperatures. Finally, the variation on DRI with temperature almost copied that for S_{20}, and so variation with temperature of DRI is more influenced by S_{20} than by SJ.

We have explored different correlations to predict the variation in the drillability with temperature from variations in the physical and mechanical properties. In this study, those correlations providing coefficients of determination greater than 0.80 and relative errors smaller than 10% have been considered. Logarithmic functions were predominant for SJ predictions, and the best correlations at high temperatures were found from UCS and Poisson's ratio for all cooling methods, and from P- and S-wave velocities for water-cooled samples. SJ predictions from UCS showed good values of relative error for the highest temperatures, but a low coefficient of determination was measured for water-cooled samples, although it strongly improved when skipping UCS value at 200 °C (R^2 = 0.99). This good correlation with UCS can be explained as vertical pressure on the bit and bit rotational speed (represented by SJ value), which have proven to be the most significant parameters in the penetration rate for rotary drilling [7]. In addition, SJ represents surface hardness [49], and therefore good correlations with UCS and other tests measuring surface hardness in the intact rock, such as Schmidt hardness test [6,53], have been observed. Su et al. [13] stated that elastic or plastic deformations affect rotary drilling, and this explains correlations with deformational parameters obtained in our research. Correlation with elastic modulus was weaker than with UCS, which is consistent with conclusions from other researchers [11,13]. Finally, good correlations with P- and S-wave velocities were previously reported in existing research [12] being higher for water-cooled samples in this case study. Coefficients of determination and residuals were remarkably better for S_{20} predictions and linear functions were predominant, providing good predictions for all variables and cooling methods. Correlations with UCS were the weakest when compared with the other parameters. It should be pointed out here that Dahl et al. [49] explained this result by the fact that S_{20} and UCS are two very different test methods for determining the strength properties of rock, since S_{20} is determined by applying repeated impacts on the sample material, causing crushing of the sample material, while UCS is performed by applying load on the sample, at a relatively slow constant rate, until failure occurs.

The correlations between SJ and S_{20} with physical and mechanical parameters in thermally treated rocks derived from this work showed greater coefficients of determination than those reported for intact rocks by most authors [11–13]. The reason could be related to the fact that the increase in thermal damage in the rock (in terms of porosity and micro crack growth and coalescence), especially at certain temperatures, proportionally affects all the studied properties from Prada limestone. An increase in the micro-fissures leads to an increase in the ability to indent represented by SJ, and a drop in the rock resistance to crushing represented by S_{20}. In other words, variability in the studied properties from Prada limestone is caused by common thermal damage phenomena. Indeed, thermal treatment induces thermal decay on limestones, and that is triggered by well-known processes such as the decomposition of clay minerals cementing particles or filling micropores [26]. For temperatures of up to 200 °C, the loss of water is the main influencing factor in the thermal damage of limestones [26] due to high-pressure vapour escaping from the rock sample that causes the generation and coalescence of micro-fractures [54].

Quartz-bearing limestones experiment a dramatic microcracking and volume increase at the phase transition between 550 and 600 °C, with a strong peak at 573 °C [30,31]. Local thermal stress concentrations and microcracking occur due to mismatches in thermal expansion coefficients of different mineral particles [25,55–57], especially in the range of temperatures between 400 and 500 °C [54]; and thermal oxidation of pyrites leads to a dramatic increase in pore-pressure on pyrite-bearing limestones, resulting in increased thermal damage and explosive behaviour [23]. All these processes affect rock integrity and cause a continuous and gradual decay in physical and mechanical properties of rock with temperature—with some threshold temperatures marking changes in the general trend [54]. For all the above, it can be stated that strong correlations between physical, mechanical, and drillability variables in thermally treated Prada limestone can be explained by a common pattern of change in features due to thermal damage processes.

Consequently, the strong correlations observed between UCS and SJ, and between P- and S-wave velocities and S_{20}, enable quick and easy evaluations to be made of the variation with temperature in drillability based on the variation of such mechanical and physical properties for supporting tunnel excavations. Furthermore, these results open the door to the development of drilling and excavation equipment based on the concept of thermal treatments for improving the tunnel excavation performance.

5. Conclusions

In our study, samples from Prada limestone were heated to temperatures of 105, 200, 300, 400, 500, and 600 °C and then cooled at a slow rate in air, or by quenching in water. The rocks significantly increased in surface hardness, resistance to indentation (measured by Siever's J value), and in brittleness (measured by the brittleness S_{20} value). These measurements combined with the evidence from the DRI index, point to a sustained increase in rock drillability. Variation in drillability with temperature were compared with decay in mechanical (UCS, elastic modulus and Poisson's ratio) and physical (P- and S-wave velocity) properties of Prada limestone. The derived conclusions of our study are listed below:

1. DRI increased with temperature, implying a change in the drillability category at 500 °C (from medium to high) and a total increase of 40% at 600 °C, with no significant differences between cooling methods in the studied range of temperatures.
2. A decrease in DRI at 200 °C for water-cooled samples is explained by the closure of pores and fissures at that temperature.
3. Temperature influence is remarkable, as SJ tripled and S_{20} doubled at 600 °C the initial values for intact rock. An increase in micro-fissures leads to an increase in the ability to indent represented by SJ, and a drop in resistance to crushing represented by S_{20}.
4. DRI trend almost copied that for S_{20}, so thermal variation in DRI is more influenced by S_{20} than by SJ.
5. We investigated correlations to predict the variation of SJ and S_{20} with temperature from variations in the physical and mechanical properties, and we reported strong correlations between most of the studied variables. The common explanation for these correlations is that variation of the studied properties with temperature is caused by a common thermal damage phenomenon (increase in porosity and micro cracking growth and coalescence) that strongly affects all considered geomechanical parameters.

In summary, a substantial improvement in the drillability of the rock when heated, measured in terms of DRI value increase, can help improve the efficiency of mechanical excavation. Additionally, the obtained correlations enable quick and easy evaluations of drillability based on basic geomechanical parameters (such as UCS and P- and S-velocities) to support the Tres Ponts Tunnel excavations.

Author Contributions: Conceptualization, V.M.-I., M.E.G., C.H.S., T.M. and R.T.; Data curation, C.H.S. and A.B.; Formal analysis, V.M.-I.; Methodology, V.M.-I., M.E.G., C.H.S. and A.B.; Supervision, T.M. and R.T.; Writing—original draft, V.M.-I.; Writing—review & editing, M.E.G., C.H.S., T.M. and R.T. All authors have read and agreed to the published version of the manuscript.

Funding: This research received no external funding.

Institutional Review Board Statement: Not applicable.

Informed Consent Statement: Not applicable.

Data Availability Statement: Data is contained within the article.

Acknowledgments: The authors wish to acknowledge David Benavente and Juan Carlos Cañaveras from the University of Alicante, for their valuable help on mineralogical and petrographic description of the rock. Additionally, Kreum SA, Ayesa SA, Infraestructures de la Generalitat de Catalunya, S.A.U., and the Lleida regional roads authority (Servei Territorial de Carreteres de Lleida, Generalitat de Catalunya) for providing rock samples. This work was supported by the Department of Geological and Geotechnical Engineering, Universitat Politècnica de València.

Conflicts of Interest: The authors declare no conflict of interest.

References

1. Yetkin, M.E.; Özfırat, M.K.; Yenice, H.; Şimşir, F.; Kahraman, B. Examining the relation between rock mass cuttability index and rock drilling properties. *J. Afr. Earth Sci.* **2016**, *124*, 151–158. [CrossRef]
2. Yaşar, E.; Ranjith, P.G.; Viete, D.R. An experimental investigation into the drilling and physico-mechanical properties of a rock-like brittle material. *J. Pet. Sci. Eng.* **2011**, *76*, 185–193. [CrossRef]
3. Yarali, O.; Kahraman, S. The drillability assessment of rocks using the different brittleness values. *Tunn. Undergr. Space Technol.* **2011**, *26*, 406–414. [CrossRef]
4. Altindag, R. Assessment of some brittleness indexes in rock-drilling efficiency. *Rock Mech. Rock Eng.* **2010**, *43*, 361–370. [CrossRef]
5. Yarali, O.; Soyer, E. The effect of mechanical rock properties and brittleness on drillability. *Sci. Res. Essays* **2011**, *6*, 1077–1088. [CrossRef]
6. Yarali, O.; Soyer, E. Assessment of relationships between drilling rate index and mechanical properties of rocks. *Tunn. Undergr. Space Technol.* **2013**, *33*, 46–53. [CrossRef]
7. Saeidi, O.; Torabi, S.R.; Ataei, M.; Rostami, J. A stochastic penetration rate model for rotary drilling in surface mines. *Int. J. Rock Mech. Min. Sci.* **2014**, *68*, 55–65. [CrossRef]
8. Özfırat, M.K.; Yenice, H.; Şimşir, F.; Yaralı, O. A new approach to rock brittleness and its usability at prediction of drillability. *J. Afr. Earth Sci.* **2016**, *119*, 94–101. [CrossRef]
9. Capik, M.; Yilmaz, A.O.; Yasar, S. Relationships between the drilling rate index and physicomechanical rock properties. *Bull. Eng. Geol. Environ.* **2017**, *76*, 253–261. [CrossRef]
10. Yenice, H. Determination of Drilling Rate Index Based on Rock Strength Using Regression Analysis. *An. Acad. Bras. Cienc.* **2019**, *91*, 1–10. [CrossRef]
11. Jamshidi, E.; Arabjamaloei, R.; Hashemi, A.; Ekramzadeh, M.A.; Amani, M. Real-time Estimation of Elastic Properties of Formation Rocks Based on Drilling Data by Using an Artificial Neural Network. *Energy Sources Part A Recover. Util. Environ. Eff.* **2013**, *35*, 337–351. [CrossRef]
12. Ataei, M.; KaKaie, R.; Ghavidel, M.; Saeidi, O. Drilling rate prediction of an open pit mine using the rock mass drillability index. *Int. J. Rock Mech. Min. Sci.* **2015**, *73*, 130–138. [CrossRef]
13. Su, O.; Sakız, U.; Akçın, N.A. Effect of elastic and strength properties of rocks during blasthole drilling. In Proceedings of the ISRM International Symposium-EUROCK 2016, Cappadocia, Turkey, 29–31 August 2016; pp. 217–221. [CrossRef]
14. Martinho, E.; Dionísio, A. Assessment Techniques for Studying the Effects of Fire on Stone Materials: A Literature Review. *Int. J. Archit. Herit.* **2020**, *14*, 275–299. [CrossRef]
15. Lion, M.; Skoczylas, F.; Ledésert, B. Effects of heating on the hydraulic and poroelastic properties of bourgogne limestone. *Int. J. Rock Mech. Min. Sci.* **2005**, *42*, 508–520. [CrossRef]
16. Yavuz, H.; Demirdag, S.; Caran, S. Thermal effect on the physical properties of carbonate rocks. *Int. J. Rock Mech. Min. Sci.* **2010**, *47*, 94–103. [CrossRef]
17. Franzoni, E.; Sassoni, E.; Scherer, G.W.; Naidu, S. Artificial weathering of stone by heating. *J. Cult. Herit.* **2013**, *14*, e85–e93. [CrossRef]
18. Brotóns, V.; Tomás, R.; Ivorra, S.; Alarcón, J.C. Temperature influence on the physical and mechanical properties of a porous rock: San Julian's calcarenite. *Eng. Geol.* **2013**, *167*, 117–127. [CrossRef]
19. Andriani, G.F.; Germinario, L. Thermal decay of carbonate dimension stones: Fabric, physical and mechanical changes. *Environ. Earth Sci.* **2014**, *72*, 2523–2539. [CrossRef]
20. Sengun, N. Influence of thermal damage on the physical and mechanical properties of carbonate rocks. *Arab. J. Geosci.* **2014**, *7*, 5543–5551. [CrossRef]
21. Mao, X.-B.; Zhang, L.; Li, T.; Liu, H. Properties of failure mode and thermal damage for limestone at high temperature. *Min. Sci. Technol.* **2009**, *19*, 290–294. [CrossRef]
22. Beck, K.; Janvier-Badosa, S.; Brunetaud, X.; Török, Á.; Al-Mukhtar, M. Non-destructive diagnosis by colorimetry of building stone subjected to high temperatures. *Eur. J. Environ. Civ. Eng.* **2016**, *20*, 643–655. [CrossRef]
23. Martínez-Ibáñez, V.; Benavente, D.; Hidalgo Signes, C.; Tomás, R.; Garrido, M.E.E. Temperature-Induced Explosive Behaviour and Thermo-Chemical Damage on Pyrite-Bearing Limestones: Causes and Mechanisms. *Rock Mech. Rock Eng.* **2021**, *54*, 219–234. [CrossRef]
24. Ozguven, A.; Ozcelik, Y. Investigation of some property changes of natural building stones exposed to fire and high heat. *Constr. Build. Mater.* **2013**, *38*, 813–821. [CrossRef]
25. Zhang, W.; Sun, Q.; Zhu, S.; Wang, B. Experimental study on mechanical and porous characteristics of limestone affected by high temperature. *Appl. Therm. Eng.* **2017**, *110*, 356–362. [CrossRef]
26. Zhang, W.; Lv, C. Effects of mineral content on limestone properties with exposure to different temperatures. *J. Pet. Sci. Eng.* **2020**, *188*, 106941. [CrossRef]
27. Martínez-Ibáñez, V.; Garrido, M.E.; Hidalgo Signes, C.; Tomás, R. Micro and macro-structural effects of high temperatures in Prada limestone: Key factors for future fire-intervention protocols in Tres Ponts Tunnel (Spain). *Constr. Build. Mater.* **2021**, *286*, 122960. [CrossRef]

28. Malaga-Starzec, K.; Åkesson, U.; Lindqvist, J.E.; Schouenborg, B. Microscopic and macroscopic characterization of the porosity of marble as a function of temperature and impregnation. *Constr. Build. Mater.* **2006**, *20*, 939–947. [CrossRef]
29. Belmokhtar, M.; Delage, P.; Ghabezloo, S.; Conil, N. Thermal Volume Changes and Creep in the Callovo-Oxfordian Claystone. *Rock Mech. Rock Eng.* **2017**, *50*, 2297–2309. [CrossRef]
30. Glover, P.W.J.; Baud, P.; Darot, M.; Meredith, P.G.; Boon, S.A.; LeRavalec, M.; Zoussi, S.; Reuschlé, T. α/β phase transition in quartz monitored using acoustic emissions. *Geophys. J. Int.* **1995**, *120*, 775–782. [CrossRef]
31. Van der Molen, I. The shift of the α-β transition temperature of quartz associated with the thermal expansion of granite at high pressure. *Tectonophysics* **1981**, *73*, 323–342. [CrossRef]
32. Mallet, C.; Fortin, J.; Guéguen, Y.; Bouyer, F. Evolution of the crack network in glass samples submitted to brittle creep conditions. *Int. J. Fract.* **2014**, *190*, 111–124. [CrossRef]
33. Kubik, M. *The Future of Geothermal Energy*; Massachusetts Institute of Technology: Cambridge, MA, USA, 2006; ISBN 0615134386.
34. Sigfusson, B.; Uihlein, A. *2014 JRC Geothermal Energy Status Report*; Joint Research Centre, Ed.; European Union: Petten, The Netherlands, 2015; ISBN 9789279446146.
35. Rossi, E.; Kant, M.A.; Madonna, C.; Saar, M.O.; Rudolf von Rohr, P. The Effects of High Heating Rate and High Temperature on the Rock Strength: Feasibility Study of a Thermally Assisted Drilling Method. *Rock Mech. Rock Eng.* **2018**, *51*, 2957–2964. [CrossRef]
36. Jamali, S.; Wittig, V.; Börner, J.; Bracke, R.; Ostendorf, A. Application of high powered Laser Technology to alter hard rock properties towards lower strength materials for more efficient drilling, mining, and Geothermal Energy production. *Geomech. Energy Environ.* **2019**, *20*, 100112. [CrossRef]
37. Rossi, E.; Saar, M.O.; Rudolf von Rohr, P. The influence of thermal treatment on rock–bit interaction: A study of a combined thermo–mechanical drilling (CTMD) concept. *Geotherm. Energy* **2020**, *8*, 16. [CrossRef]
38. Rossi, E.; Jamali, S.; Wittig, V.; Saar, M.O.; Rudolf von Rohr, P. A combined thermo-mechanical drilling technology for deep geothermal and hard rock reservoirs. *Geothermics* **2020**, *85*, 101771. [CrossRef]
39. Rossi, E.; Jamali, S.; Saar, M.O.; Rudolf von Rohr, P. Field test of a Combined Thermo-Mechanical Drilling technology. ModeI: Thermal spallation drilling. *J. Pet. Sci. Eng.* **2020**, *190*, 107005. [CrossRef]
40. Rossi, E.; Jamali, S.; Schwarz, D.; Saar, M.O.; Rudolf von Rohr, P. Field test of a Combined Thermo-Mechanical Drilling technology. Mode II: Flame-assisted rotary drilling. *J. Pet. Sci. Eng.* **2020**, *190*, 106880. [CrossRef]
41. Bruland, A. Hard Rock Tunnel Boring: Vol. 8 Drillability Test Methods. Ph.D. Thesis, Norwegian University of Science and Technology, Trondheim, Norway, 2000.
42. Dahl, F.; Grøv, E.; Bruland, A.; Nilsen, B. Trademarking the NTNU/SINTEF drillability test indices. *Tunnels Tunn. Int.* **2010**, 44–46.
43. von Matern, N.; Hjelmér, A. *Försök med Pågrus ("Tests with Chippings")*; Statens väginstitut: Stockholm, Sweden, 1943.
44. Sievers, H. Die Bestimmung des Bohrwiderstandes von Gesteinen. In *Proceedings of the Glückauf*; Glückauf G.M.B.H: Essen, Germany, 1950; Volume 86, pp. 776–784.
45. Hartman, H.L. Basic Studies of Percussion Drilling. *Min. Eng.* **1959**, *11*, 68–75.
46. Kahraman, S.; Bilgin, N.; Feridunoglu, C. Dominant rock properties affecting the penetration rate of percussive drills. *Int. J. Rock Mech. Min. Sci.* **2003**, *40*, 711–723. [CrossRef]
47. Hoseinie, S.H.; Ataei, M.; Osanloo, M. A new classification system for evaluating rock penetrability. *Int. J. Rock Mech. Min. Sci.* **2009**, *46*, 1329–1340. [CrossRef]
48. Kahraman, S. Rotary and percussive drilling prediction using regression analysis. *Int. J. Rock Mech. Min. Sci.* **1999**, *36*, 981–989. [CrossRef]
49. Dahl, F.; Bruland, A.; Jakobsen, P.D.; Nilsen, B.; Grøv, E. Classifications of properties influencing the drillability of rocks, based on the NTNU/SINTEF test method. *Tunn. Undergr. Space Technol.* **2012**, *28*, 150–158. [CrossRef]
50. Nasseri, M.H.B.; Schubnel, A.; Young, R.P. Coupled evolutions of fracture toughness and elastic wave velocities at high crack density in thermally treated Westerly granite. *Int. J. Rock Mech. Min. Sci.* **2007**, *44*, 601–616. [CrossRef]
51. Martínez-Ibáñez, V.; Garrido, M.E.; Signes, C.H.; Tomás, R. Indirect Evaluation of Strength for Limestones Subjected to High Temperatures. In Proceedings of the ISRM International Symposium-EUROCK 2020, Trondheim, Norway, 12–14 October 2020.
52. Fioretti, G.; Mazzoleni, P.; Acquafredda, P.; Andriani, G.F. On the technical properties of the Carovigno stone from Apulia (Italy): Physical characterization and decay effects by means of experimental ageing tests. *Environ. Earth Sci.* **2018**, *77*, 17. [CrossRef]
53. Sabatakakis, N.; Koukis, G.; Tsiambaos, G.; Papanakli, S. Index properties and strength variation controlled by microstructure for sedimentary rocks. *Eng. Geol.* **2008**, *97*, 80–90. [CrossRef]
54. Meng, Q.-B.; Wang, C.-K.; Liu, J.-F.; Zhang, M.-W.; Lu, M.-M.; Wu, Y. Physical and micro-structural characteristics of limestone after high temperature exposure. *Bull. Eng. Geol. Environ.* **2020**, *79*, 1259–1274. [CrossRef]
55. Liu, S.; Xu, J. Study on dynamic characteristics of marble under impact loading and high temperature. *Int. J. Rock Mech. Min. Sci.* **2013**, *62*, 51–58. [CrossRef]
56. Yang, J.; Fu, L.-Y.; Zhang, W.; Wang, Z. Mechanical property and thermal damage factor of limestone at high temperature. *Int. J. Rock Mech. Min. Sci.* **2019**, *117*, 11–19. [CrossRef]
57. Villarraga, C.J.; Gasc-Barbier, M.; Vaunat, J.; Darrozes, J. The effect of thermal cycles on limestone mechanical degradation. *Int. J. Rock Mech. Min. Sci.* **2018**, *109*, 115–123. [CrossRef]